PAN ARCHIVES OF ACOUSTICS
Vol. **41**, No. 2, pp. 285–296 (2016)

DOI: 10.1515/aoa-2016-0028

Vibroacoustic Measurements and Simulations Applied to External Gear Pumps. An Integrated Simplified Approach

Eleonora CARLETTI, Giuseppe MICCOLI, Francesca PEDRIELLI, Giorgio PARISE

C.N.R.-IMAMOTER
Institute for Agricultural and Earthmoving Machines of the National Research Council of Italy
Via Canal Bianco, 28 – 44124 Ferrara, Italy; e-mail: e.carletti@imamoter.cnr.it

(*received March 24, 2016; accepted April 4, 2016*)

This paper describes the development phases of a numerical-experimental integrated approach aimed at obtaining sufficiently accurate predictions of the noise field emitted by an external gear pump by means of some vibration measurements on its external casing. Harmonic response methods and vibroacoustic analyses were considered as the main tools of this methodology. FFT acceleration spectra were experimentally acquired only in some positions of a 8.5 cc/rev external gear pump casing for some working conditions and considered as external excitation boundary conditions for a FE quite simplified vibroacoustic model. The emitted noise field was computed considering the pump as a 'black box', without taking into account the complex dynamics of the gear tooth meshing process and the consequent fluid pressure and load distribution. Sound power tests, based on sound intensity measurements, as well as sound pressure measurements in some positions around the pump casing were performed for validation purposes. The comparisons between numerical and experimental results confirmed the potentiality of this approach in offering a good compromise between noise prediction accuracy and reduction of experimental and modelling requirements.

Keywords: airborne noise; gear pump; vibroacoustic modelling.

1. Introduction

External gear pumps are simple and robust hydraulic components, suitable to work at a wide range of pressures and rotational speeds. They have long life, high reliability and efficiency, small size, low weight, low cost and need minimum maintenance. All these features make gear pumps widely used for energy transmission in hydraulic and fluid power systems on different kinds of machines and vehicles. Unfortunately, the main drawback is their noise emission, which often affects the overall noise emission of the machines which these components are mounted in.

The public awareness with respect to the noise pollution problem has driven the publication of several regulations which establish lower noise emission limits for machinery and vehicles, making noise and vibration reduction a challenging aspect to be considered. As a consequence, also the manufacturers of hydraulic components have been forced to a more accurate evaluation of the noise emitted by their products, fundamentally for competitiveness needs.

In this context, methodologies and tools integrating vibroacoustic modelling and experimental analyses have been developed in the last decade with many different purposes:

- improving the know-how about the dynamic behaviour of these systems;
- having useful tools for the identification of noise and vibration sources;
- predicting the effects of each design modification;
- reducing the number of the tests required for the prototype development.

Many studies can be found in bibliography concerning the development of complex numerical model for the prediction of the dynamic behaviour of external gear pumps (Mucchi *et al.*, 2011; 2014; Liping *et al.*, 2011; Ragunhatan, Manoharan, 2012). The development of these models, however, turns out to be a very demanding task and requires an accurate analysis of the system, the definition of the most important phenomena as well as their formulation in order to simultaneously fulfil the model goals and the

numerical constraints (Sandberg, Ohayon, 2009). In addition, very long calculation times and significant computational means are required (Margetts, 2015; Vansant *et al.*, 2014; Bériot *et al.*, 2013; Raju, Khaitan, 2012). In return to so many resources and efforts, the outcome is a very powerful tool, able to study the effects of relevant pump design parameters such as gear characteristics (profile, shape, material and errors) and other relevant parts (input and output chambers, transportation arc, lateral plates grooves, bearing blocks, etc.) (Mucchi *et al.*, 2010a; 2010b; Opperwall, Vacca, 2014).

This work describes the different development phases of a more simplified pump vibroacoustic model. The purpose consists in achieving a numerical-experimental integrated approach, applicable at industrial level, able to predict the noise field emitted by a gear pump with a sufficient accuracy, by means of few vibration measurements on the pump external casing. This methodology was developed for an external gear pump, considered as a 'black box' in order to disregard all the complex phenomena characterizing its working process. In the following paragraphs the main phases are described in detail concerning the definition of the FE structural model, the structural analyses, the BE vibroacoustic model and related analyses, as well as the different experimental tests carried out for validation purposes.

2. Airborne noise generation in external gear pumps

Gear pumps are components mainly used in hydraulic and fluid power systems for energy transmission. They consist of two meshing spur gears, usually with 9 to 12 teeth, enclosed in a closely fitting casing. One gear is driven by a motor and in turn it drives the other one. The simplest version has straight cut 'spur' gear teeth of involute form but 'herring bone' and 'helical form' teeth are also available. The two gears are supported by two lateral hollow bushes and two bearings. The bearings allow the gears to rotate at high shaft speed and different seals are placed inside the bushes in order to prevent fluid leakages (Skaistis, 1988).

As these meshed teeth separate, they create a partial vacuum which is filled by the fluid being pumped. As the gears continue to rotate, the fluid becomes trapped and is pushed around the casing to the discharge side of the pump (Fig. 1).

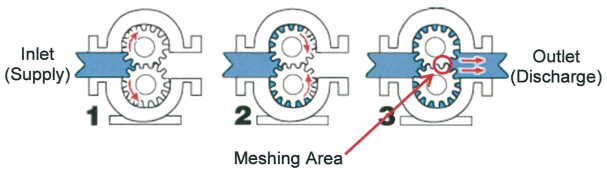

Fig. 1. Scheme of operation of an external gear pump.

The pumping operation which takes place in the meshing area produces noise at the gear meshing frequency and related harmonics. The fundamental frequency is calculated by Eq. (1):

$$f_m = \frac{n_{\text{teeth}} \cdot \omega}{60}, \tag{1}$$

where n_{teeth} is the number of teeth and ω is the shaft rotational speed (rpm).

On the other hand, the pressure fluctuations generated in the fluid induce vibrations on the mechanical parts. When the frequencies of these vibrations coincide with the natural vibration modes of these parts, they resonate and can act as acoustic radiators themselves, generating airborne noise. The actual entity of the emitted airborne noise finally depends on the dynamic characteristics of the system and the acoustic coupling between the vibrating surfaces and the surrounding medium (air). In addition, even the not perfect balance of the rotating parts or their eccentricity may generate vibrations and therefore airborne noise.

The simplicity of the mechanical parts composing a gear pump (Fig. 2) could lead to misleading deductions. In spite of this minimal assembly, indeed, the design and the analysis of this hydraulic component is far from being simple, because more functional roles are associated with its individual parts and consequently the overall dynamic behaviour consists in the complex combination of multiple effects.

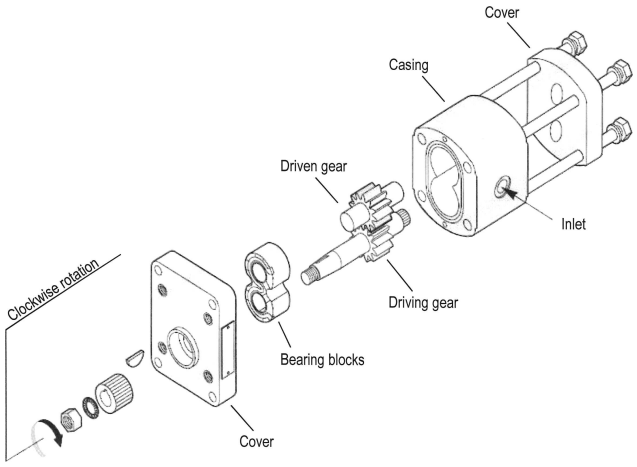

Fig. 2. Exploded view of an external gear pump.

Several factors contribute to the noise emission of a gear pump:

- the pressure distribution inside the vanes between gear teeth;
- the reactions of the constraint of the hydrodynamic bearings;
- the clearances between the gears, between the gears and the casing, between the gear axes and the bushes;

- the physical-mechanical properties of the fluid (temperature, viscosity, ...);
- the outlet pressure;
- the shaft speed of the engine;
- the number and the shape of the teeth.

For several decades detailed and extensive studies have been carried out on this type of equipment in order to study the effects of the above factors on the emitted airborne noise. In particular, papers can be found dealing with the effects due to the time-varying oil pressure distribution on the gears and the time-varying meshing stiffness (Kuang, Lin, 2002; Stryczek *et al.*, 2015) or the displacement volumes (Huang *et al.*, 2008); the effects due to the teeth (Wojnarowski, Onishchenko, 2003), the tooth number and profile errors (Manring, Kasaragadda, 2003; Pedrielli, Carletti, 2014) or the tooth material (Rodionov *et al.*, 2015); the effects due to the journal bearings misalignment and bearing blocks (Bonanno, Pedrielli, 2008; Borghi *et al.*, 2008), to the axial balance (Borghi *et al.*, 2005) or to the eccentricity between gear and housing (Sung-Hoon *et al.*, 2013); the effects due to the viscosity of the fluid (Stupa, Chernyshov, 1990). Despite this large bibliography, the formulation of the dynamic behaviour of this kind of pumps is still a demanding task due to the complexity of the several contributions and mutual interactions.

3. Experiments

A 8.5 cc/rev external gear pump with 12 tooth gear set was chosen for this study. The development of the pump simulation model as well as the phases of the validation process involved different types of measurements, such as acceleration waterfall spectra acquired at variable shaft speed, acceleration and sound pressure spectra measured at different working conditions, sound power spectra obtained by sound intensity measurements.

3.1. The test rig

The data acquisition was performed in laboratory using a test rig built to comply with the mounting conditions suggested by ISO 16902-1. This standard is specifically addressed to the sound power tests based on sound intensity measurements but the conditions of installation and operation of the pump were suitable also for the vibration measurements.

As shown in Fig. 3, the mounting arrangement included one reflecting plane (concrete wall) coincident with the mounting face of the pump and placed in between the pump supporting flange and the prime mover. The inlet and the discharge pipes were passing through this reflecting plane. The hydraulic circuit included oil filters, oil coolers, restrictor valves and a reservoir as required in order to conform to the pump hydraulic operating conditions. All these elements were placed behind the concrete wall so that the noise radia

ISO 16902-1:2003(E)

Key

1 piping
2 pump under test
3 measurement surface
4 soft rubber seal
5 prime mover
6 reflecting plane
7 reflecting plane isolated from the support frame

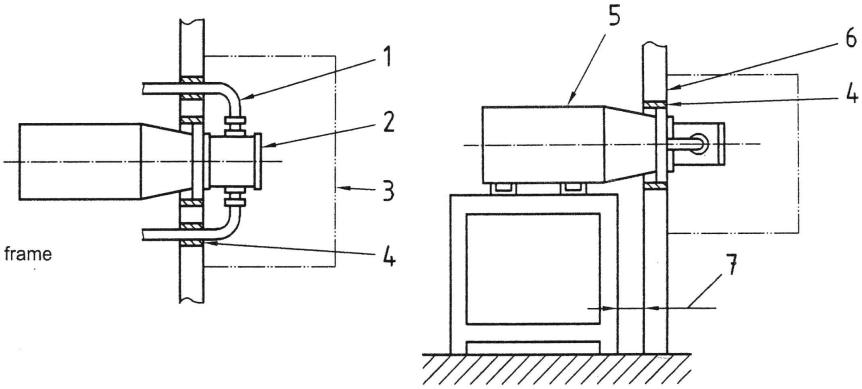

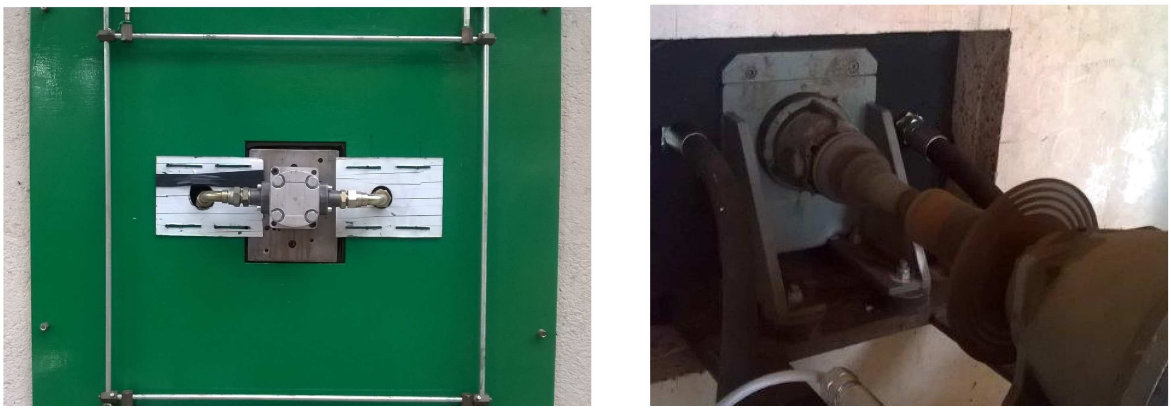

Fig. 3. Test rig used for sound and vibration measurements.

ted was as low as possible. Different transducers (oil pressure, oil temperature, flow and shaft speed) were integrated in the circuit in order to permit a continuous monitoring of all the variables during the data acquisitions. This check ensured the repeatability of the operating conditions of the source under test.

Most of the sound and vibration measurements were repeated at three different operating conditions, with the aim to check the methodology at different working pressures and rotational speeds. Table 1 summarises these measurement configurations.

Table 1. Measurement configurations.

Configuration	Shaft speed [rpm]	Outlet pressure [bar]	Oil temperature [°C]
A	1500	50	70
B	1500	150	70
C	2500	50	70

In addition, acceleration waterfalls were measured in different positions on the pump surface at a variable pump speed and at a fixed outlet pressure of 50 bar.

3.2. Vibration measurements

Referring to vibration measurements, different positions were selected both on the pump casing surface and on the support structure, the choice being mainly driven by our expertise in experimental analyses on this kind of hydraulic components (Carletti, Pedrielli, 2014). Figure 4 shows the 8 positions chosen for the experiments. All the measurements were carried out using both tri-axial and mono-axial accelerometers in the frequency range 0–6400 Hz, 1 Hz step.

For each position, two different types of vibration measurements were performed:

- acceleration FFT spectra at variable pump speed (acceleration ramps) from 1000 rpm to 2000 rpm, step 10 rpm, at the mean outlet pressure of 50 bar. These measurements were aimed at experimentally identifying the highest number of resonance modal frequencies of the system.
- acceleration FFT spectra in each of the operating conditions summarised in Table 1. These measurements were used to establish different sets of boundary conditions for the FE structural model.

Figure 5 shows an example of acceleration ramp acquired on position #1 (Fig. 4). The visualization as waterfall permits to plot 3 variables in just one 2D-graph. It shows indeed the variation of the acceleration values (different colours) versus frequency (abscissa) and shaft speed (ordinate).

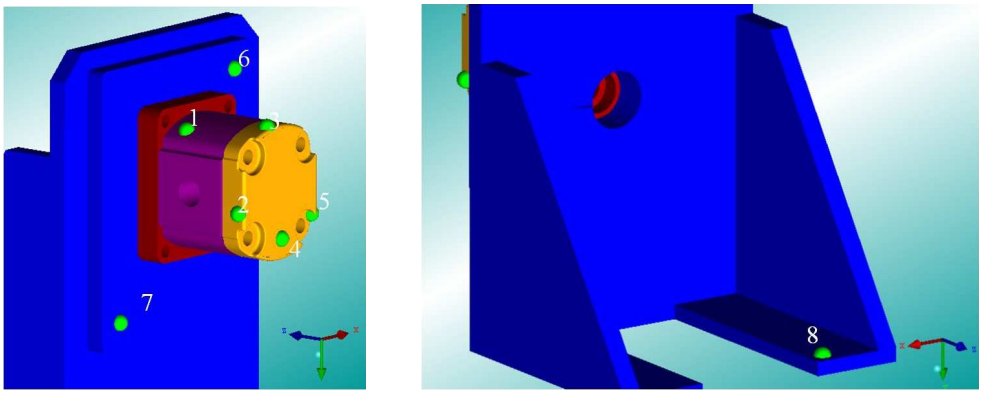

Fig. 4. The eight accelerometer positions for vibration measurements.

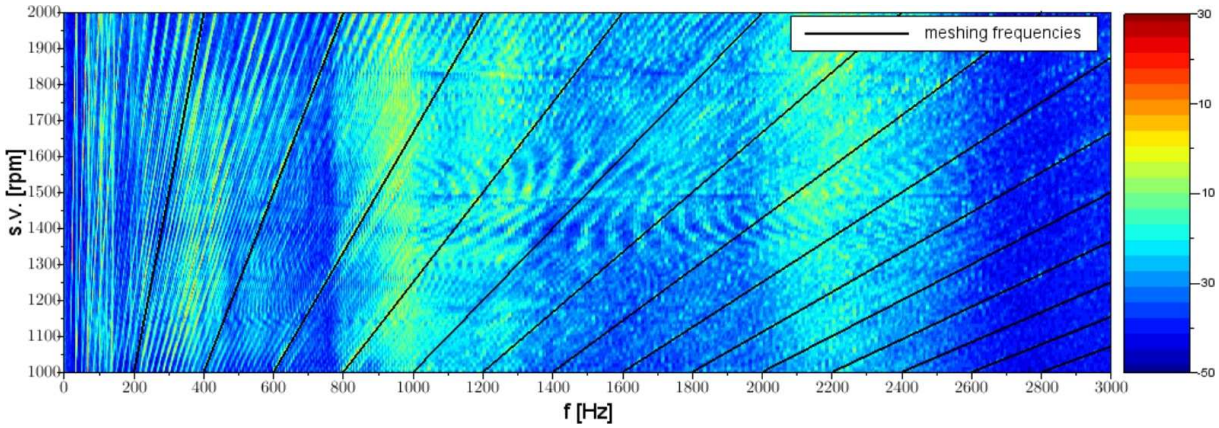

Fig. 5. Acceleration ramps at variable shaft speed measured near the pump flange.

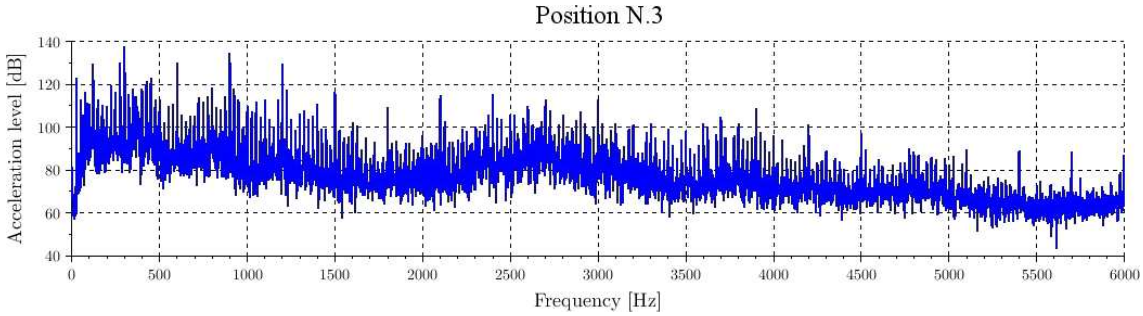

Fig. 6. Acceleration spectrum at 50 bar and 2500 rpm operating conditions.

The gear meshing and many other dynamic phenomena linearly depend on the shaft rotational speed, thus they graphically produce peaks located on inclined lines. On the other hand, the resonance modal frequencies are independent from the shaft speed, thus they produce vertical stripes, as can be seen for instance at 400 Hz, 1.25 kHz and 2.2 kHz. Other resonance frequencies were observed in other measurement positions at 250 Hz, 350 Hz, 1 kHz and 2 kHz.

Figure 6 shows an example of the acceleration spectrum acquired in the position #3, at 50 bar and 2500 rpm (configuration C). It can be seen that the amplitude of vibrations becomes less significant at frequencies higher than 4000 Hz. This gave useful indications about the frequency range of interest for this study.

3.3. Acoustic measurements

Initially, sound pressure FFT spectra were acquired in five positions around the pump for each of the three different configurations. Figure 7 shows the positions chosen around the pump for the sound pressure measurements and Fig. 8 (top) shows the corresponding setup for the measurements at the points 4 and 5.

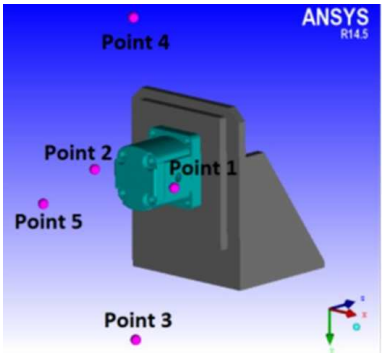

Point 1 (right)	$d = 40$ mm (positive x direction)
Point 2 (left)	$d = 40$ mm (negative x direction)
Point 3 (bottom)	$d = 200$ mm (positive y direction)
Point 4 (top)	$d = 200$ mm (negative y direction)
Point 5 (front)	$d = 200$ mm (negative z direction)

Fig. 7. Measurement positions for the sound pressure levels (d = distance from the pump surface).

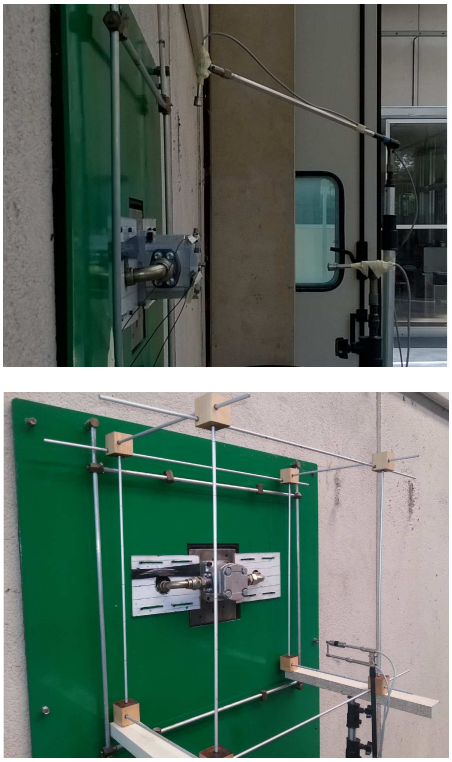

Fig. 8. Sound pressure test (top); surface and sound intensity probe for sound power test (bottom).

In general, sound pressure measurements properly describe sound waves quantitatively. However for describing the noise emission characteristics of an acoustic source, sound pressure is not a satisfactory quantity in itself as it depends on the distance between the source and the measurement position, on the environment in which the measurements are made, as well as on the presence of extraneous noise generated by sources other than that under investigation. On the other hand, the sound power emitted by noise sources represents the sound energy radiated by the source itself per unit time and therefore it has to be preferred as it is an intrinsic characteristic of the source. For these reasons, sound power tests were chosen for validation purposes.

In order to determine the sound power spectra emitted by the pump in the 3 different configurations, the method described in ISO 9614-2 was followed. This procedure is based upon sampling of the intensity field normal to the measurement surface by moving an intensity probe continuously along one or more specified paths. The component of the sound intensity vector and the mean pressure between the transducers were acquired in one-third octave bands within the range 200–5000 Hz. For each configuration, the acquisition was repeated three times in order to check the repeatability of the results.

Measurements were performed so that an engineering level of accuracy (grade 2) could be attained. This is the highest grade of accuracy that can be reached with part 2 of ISO 9614; on the other hand it was proved (Pedrielli, Carletti, 2005) that this is a good compromise between grade of accuracy that can be achieved and time-consumption. In fact, from past experience (Carletti, Pedrielli, 2005), the precision level of accuracy (grade 1) can be attained applying ISO 9614-1 only when a very fine grid of measurement points is used (around 250 points per m^2). In this case, even with an automatic positioning system of the sound intensity probe, the time necessary to complete each run is not lower than 3 hours. On the other hand, the use of ISO 9614-3 in practice never led to the desired results even if in principle it permits to reach a precision level of accuracy.

A parallelepiped ($590 \times 614 \times 348$ mm) was chosen as measurement surface, centred with respect to the pump and having one surface placed on the wall. In such a way the distance between each face of the measurement surface and the facing surface of the pump was 250 mm (in agreement with ISO 9614-2) and the pump inlet and discharge pipes were both enclosed in the measurement surface. A $7 \times 4 \times 7$ scanning path configuration was defined on the measurement surface and a manual scan was performed twice on each partial surface with a scanning speed as constant as possible. A previous study (Carletti, Pedrielli, 2006) demonstrated that the use of finer scanning path configurations may not lead to better results. Figure 8 (bottom) shows the sound power setup and the intensity probe ($1/2''$ microphones and 12 mm spacer). The measurement equipment met the requirements of class 1 instruments.

4. The numerical-experimental integrated approach

The flow chart of the work procedure for the development of the pump noise prevision methodology is shown in Fig. 9. In agreement with the final target of this study, i.e. checking the availability of a simplified numerical method in order to estimate the noise field emitted by the pump starting from vibration measure-

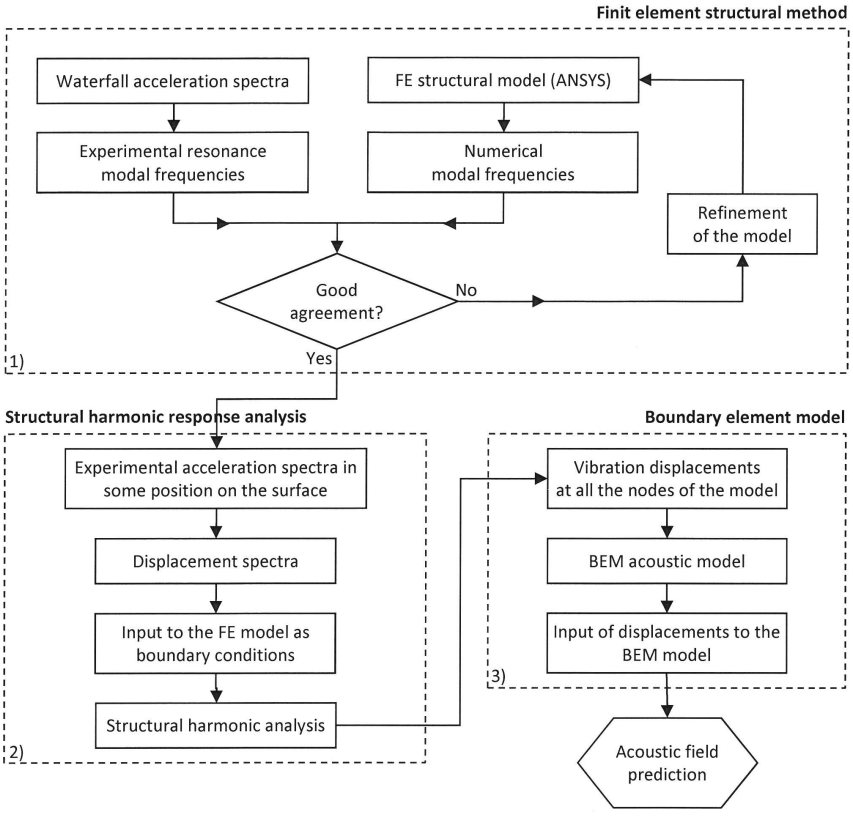

Fig. 9. Flowchart of the work procedure.

ments in some points of the pump surface, the pump under test was considered as a black-box and all the complex phenomena accompanying its working process were not taken into account.

In the flowchart three main phases can be identified:

1) the development of the FE structural model;
2) the estimate of the dynamic response of the system using only some experimental vibration spectra, acquired in different positions on the system, as boundary conditions;
3) the development of the BE vibroacoustic model and the acoustic field prediction.

4.1. The FE structural model

The initial FE structural mesh of the tested pump was obtained using the ANSYS code, taking into account the geometrical characteristics of the real system as well as the type of material (De Borst, 2012). From this initial FE model, the mode shapes and modal frequencies were calculated. Various refinement of the meshing parameters were then applied until a good agreement was reached between the numerical resonance modal frequencies and those experimentally obtained by acceleration waterfall measurements at variable shaft speed (for details on the experiments see Subsec. 3.2). In particular, the support structure was included in the pump model and this led to a significant shift of the first modal frequency from 3 kHz to 300 Hz. In addition, different materials were considered for the support structure and rigid constraints were imposed only to the support base. The final FE model consisted of 57 000 nodes and 29 000 elements of which hexahedral elements of size 14 mm for the pump support and tetrahedral elements of size 6 mm for the other parts. This final model showed about 25 different modes in the 250 Hz to 4500 Hz frequency range. Figure 10 shows the FEM mesh on the left and the table with the numerical and experimental modal frequencies, on the right (Parise *et al.*, 2015).

A suitable correlation can be found between the sets of experimental and numerical modal frequencies. Figure 11 shows two different mode shapes: mode 5

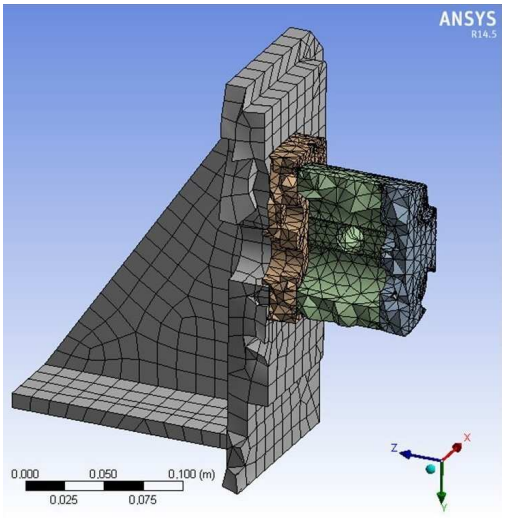

	Numerical Modal Frequencies [Hz]	Experimental Modal Frequencies [Hz]
1	262	250
2	307	350
3	667	
4	752	800
5	1037	1000
6	1059	
7	1158	1250
8	1590	
9	1602	
10	1959	2000

Fig. 10. FEM mesh (left) and numerical and experimental modal frequencies (right).

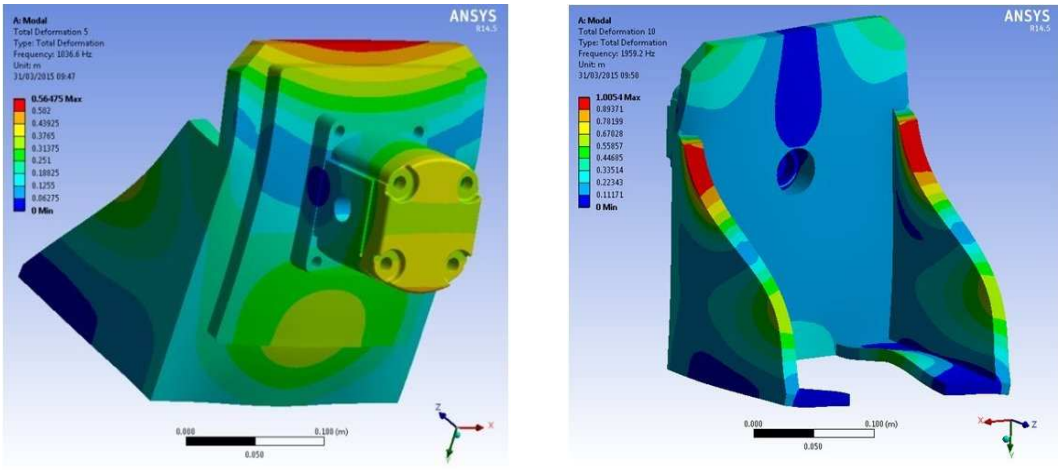

Fig. 11. Total deformation from modal analyses of mode 5, 1037 Hz (left) and mode 10, 1959 Hz (right).

at 1037 Hz (left), well related to the frequency stripe of the measured waterfall at 1000 Hz and mode 10, at 1959 Hz (right), well related to the frequency stripe of the measured waterfall at 2000 Hz.

4.2. The structural harmonic response analysis

For each of the three pump operating conditions listed in Table 1, structural harmonic analyses were performed on the FE model using the ANSYS code in order to estimate the dynamic response of the whole system. Some of the experimental acceleration spectra in the positions shown in Fig. 4 were chosen and then applied to the model as boundary conditions in terms of complex displacement spectra. The analyses were repeated for a different number of experimental vibration spectra, with the purpose to identify the minimum number of experimental data that leads to acceptable estimates of the dynamic response at all the nodes. The analyses were performed using values of the complex displacements sampled every 2 Hz, in the range 250–4500 Hz for the two operating conditions at 1500 rpm (configurations A and B) and in the range 400–4500 Hz for the operating condition at 2500 Hz (configuration C). The complex displacement spectra at all nodes of the FE model were obtained as output.

4.3. BE vibroacoustic model and sound field predictions

Starting from the FE structural model, the acoustic BE model was created using the Siemens Virtual Lab code (Miccoli *et al.*, 2012). Besides the pump it included also the inlet and discharge pipelines. The complex displacement spectra were then applied to each node of the model as boundary conditions. The BE model consisted of 3115 nodes and 6093 triangular shell elements, of 6 mm mean size. This made it possible to extend the analysis up to 8000 Hz. Figure 12 shows the BEM mesh on the left.

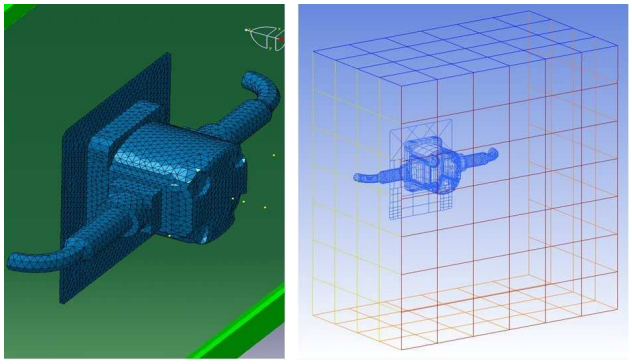

Fig. 12. BE model mesh (left) and grid of field points on the parallelepiped surface (right).

Rigid symmetry planes were then added in order to simulate the presence of the wall and the floor. Five field points were created coincident with the experimental microphones positions (Fig. 7). In addition, a grid of field points were defined on the same parallelepiped surface chosen for the experimental sound power tests (Fig. 12 right). This surface included 160 nodes and 146 quad shell elements on the whole.

All the different analyses were performed for each of the three operating conditions. The indirect variational BEM approach was chosen for the evaluations, allowing the computation of double layer potentials (jump of pressure) and single layer potentials (jump of velocity) as the results at the pump model surface. Then these surface results were post-processed in order to compute acoustic pressure, velocity and sound intensity values in the different field points or field points meshes.

5. Sound power results

Figure 13 shows the 1/3 octave band sound power spectra within the range 250–5000 Hz, obtained by sound intensity measurements for the three operating conditions.

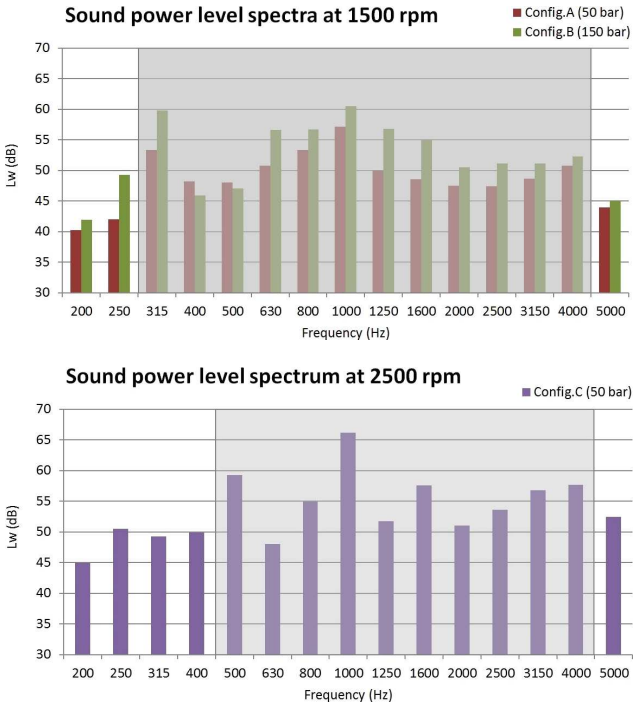

Fig. 13. Experimental sound power spectra obtained at the three operating conditions.

Using Eq. (1), the fundamental frequencies are in the 1/3 octave frequency band centred at 315 Hz for configurations A and B and in the 1/3 octave frequency band centred at 500 Hz for configuration C. As expected, the dominant levels are always at the pump characteristic frequencies, irrespective of the oil pressure and rotational speed values. Therefore the sound

power level spectra can be limited to the 315-4000 Hz frequency range (grey area in Fig. 13).

Referring to this limited frequency range, the overall sound power levels are: 62.3 dB for configuration A (50 bar at 1500 rpm), 66.5 dB for configuration B (150 bar at 1500 rpm), and 68.8 dB for configuration C (50 bar at 2500 rpm). Form these levels we can notice that configuration C is the noisiest and that the increase of the rotational speed from 1500 to 2500 rpm has an effect on the overall sound power level greater than the increase of the oil pressure from 50 to 150 bar.

6. Validation of the numerical results

For each working condition (A, B, C), numerical sound field predictions were obtained using three different sets of experimental acceleration spectra (Fig. 4):

- Set 1: three experimental acceleration spectra acquired in the positions 3-4-5 on the pump surface;
- Set 2: all the eight experimental acceleration spectra;
- Set 3: five experimental acceleration spectra acquired in the positions 1-2-3-4-5 on the pump surface.

For each case, the validation of the numerical methodology was based on the comparison between the numerical and the experimental results.

6.1. Sound field prediction based on 3 acceleration spectra (set 1)

In the first numerical test, three acceleration spectra were applied to the structural model and the complex displacement spectra, calculated in all the nodes of the FE model, were then applied to the BE vibroacoustic model as boundary conditions. The sound pressure levels were calculated in the five field points coincident with the experimental microphone positions (Fig. 7). These first analyses were repeated for the three operating conditions and were limited to the frequency range 0–3000 Hz. In such a way the simulation time was limited and, on the other hand, it was possible to compare the numerical sound pressure levels with the experimental ones at the first harmonic frequencies, where the dominant noise contributions are centred. In general, these comparisons showed that the differences between numerical and experimental data varied from −20 dB to +20 dB depending on the considered point. As an example, Fig. 14 shows the results obtained for the configuration A at the microphone position #4.

These preliminary results mainly pointed out that the use of only three experimental vibration spectra leads to sound field predictions not so accurate and that the sound pressure measurements are not very satisfactory to quantify the noise emission characteristics of a source. Due to the limited accuracy, no more tests were performed for validation purpose.

6.2. Sound field prediction based on 8 acceleration spectra (set 2)

A second numerical test was performed using the experimental acceleration spectra acquired in all the eight positions shown in Fig. 4, which included also three positions on the support structure. For each of the three operating conditions, the sound intensity field was numerically computed in the grid of field points defined on the same parallelepiped surface chosen for the experimental sound power tests (Fig. 12). The numerical analyses were performed in the range 250–4500 Hz for the two operating conditions at 1500 rpm (A, B) and in the range 400–4500 Hz for the operating condition at 2500 Hz (C). The sound power spectra were then computed for each single face (partial sound power) and for the whole parallelepiped surface (total sound power), as well.

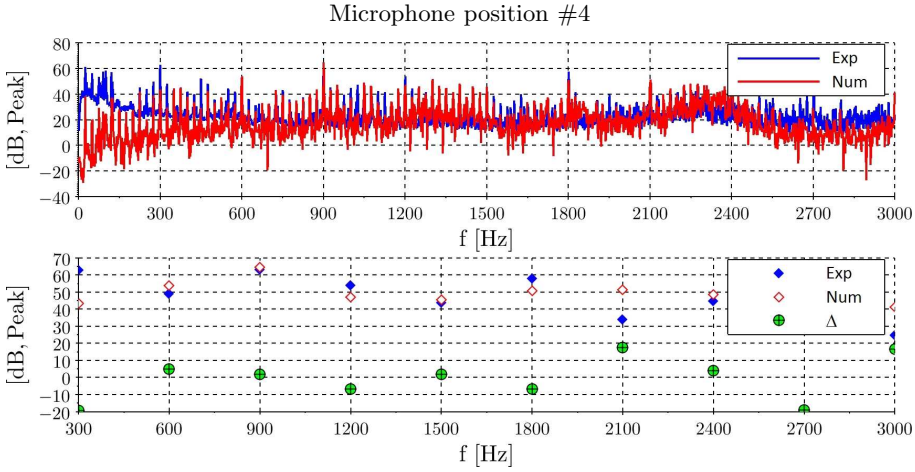

Fig. 14. Sound pressure comparisons for configuration A at the pump characteristic frequencies.

Figure 15 shows the comparisons between experimental and numerical overall sound power levels for the three operating conditions for the total sound power level (top) and for each single face (bottom).

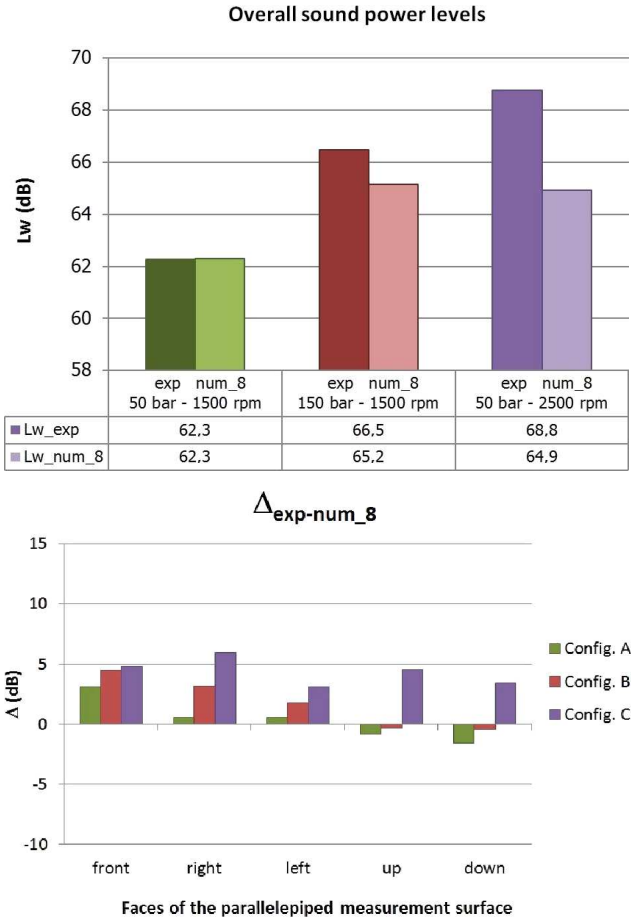

Fig. 15. Numerical and experimental results using set 2: overall sound power levels (top) – partial sound power levels (bottom).

Numerical and experimental results are very close each other. The same sound power level was obtained for configuration A, while differences of 1.3 dB and 3.9 dB were found for configurations B and C. In both these conditions, the numerical sound power levels turned out to be lower than the experimental ones. The highest differences were found for configuration C, which turns out to be the most critical working condition. The reason is that the high rotational speed induced very high vibrations on the engine shaft which could not be completely damped at the pump mounting flange. Consequently, the measured sound power spectrum (Fig. 13 bottom) showed significant noise components also at high frequencies. These effects are not related to the meshing process and could not be taken into account in the numerical approach.

In terms of partial sound power levels (Fig. 15 bottom), for configuration C the differences between experimental and numerical results are almost the same for all the faces while for the other configurations the differences can be referable mainly to the front face for configuration A and to the front and right faces for configuration B.

6.3. Sound field prediction based on 5 acceleration spectra (set 3)

Consistently with the target of this study, that is the identification of the lowest number of acceleration measurements which leads to an acceptable estimate of the noise field emitted by the pump, a further numerical test was performed using the five experimental acceleration spectra acquired on the pump surface (set 3). The same analyses as described in paragraph 6.2 were performed. Figure 16 shows the comparisons between experimental and numerical overall sound power levels for the three operating conditions, for the total sound power level (top) and for each single face (bottom).

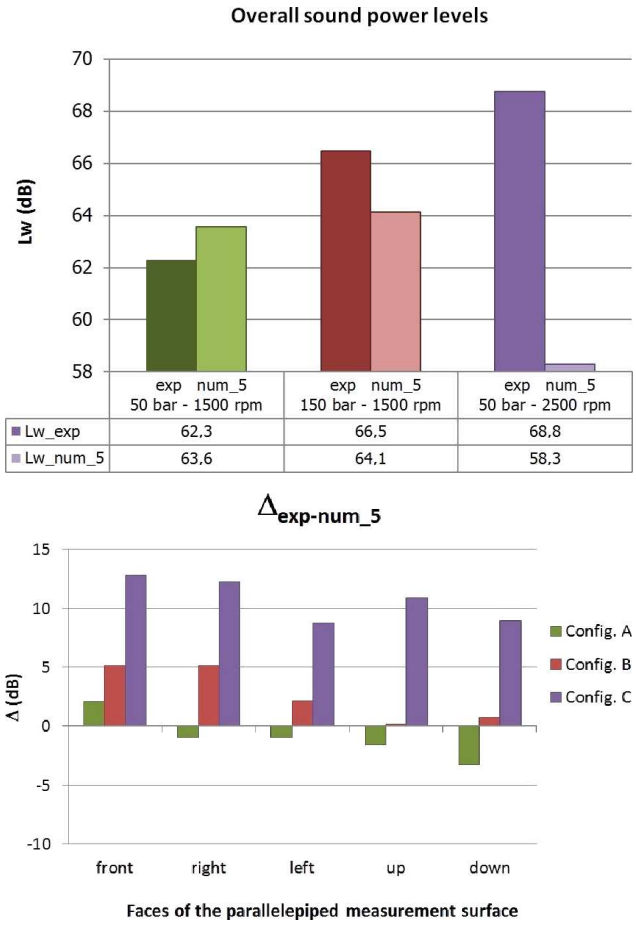

Fig. 16. Numerical and experimental results using set 3: overall sound power levels (top) – partial sound power levels (bottom).

Differences between experimental and numerical results are found for all the configurations: −1.3 dB for configuration A, +2.4 dB for configuration B and +10.5 dB for configuration C. As the difference obtained for configuration A is lower than the measure-

ment uncertainty, the results can be considered fully equivalent to those obtained using the eight acceleration spectra. The results obtained for configurations B and C confirmed the trend of this numerical approach to underestimate the emitted sound power field compared to the experimental results. The extremely high differences between experimental and numerical results for configuration C make the choice of set 3 unsatisfactory for the study purposes. However, these negative results should not be generalised as the choice of other 5 spectra, possibly including one or more positions on the support structure could better take into account the vibratory conditions and lead to better results than the current ones. Further investigations are necessary regarding this matter.

Finally, referring to the partial sound power levels (Fig. 16 bottom), the differences between experimental and numerical sound power levels are very significant for configuration C, irrespective of the considered face. For configurations A and B, on the contrary, the small differences in the overall levels have to be mainly referred to the results obtained on the front and right faces, as it was found in the second numerical test (set 2).

6.4. Final considerations

Figure 17 summarises the results of the validation tests with 8 (▲) and 5 (■) acceleration spectra at the three tested configurations A, B and C. In this graph the numerical results are plotted versus the experimental ones. The bisecting line represents the locus of points with a perfect equality between experimental and numerical values; therefore, the points closest to the bisecting line represent the best fitting. All the points above this line have numerical sound power levels higher than the experimental ones while the points below this line have numerical sound power levels lower than the experimental ones.

For each configuration, the analyses based on different sets of acceleration spectra leads to similar results if the points are close to each other.

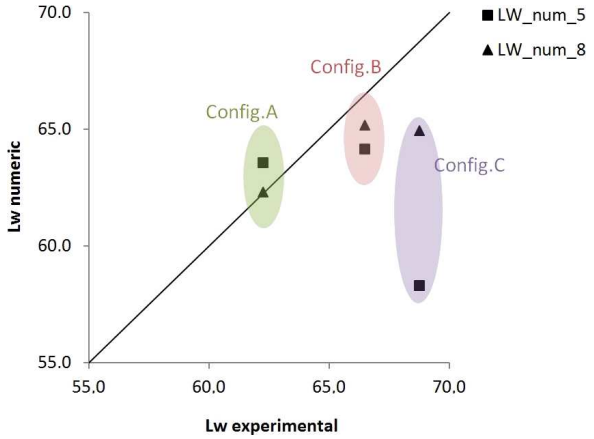

Fig. 17. Numerical and experimental results.

7. Conclusions

This paper describes the development phases of a numerical-experimental integrated approach aimed at predicting the noise field emitted by an external gear pump with sufficient accuracy, by means of some vibration measurements on its external casing. Harmonic response methods and vibroacoustic analyses were considered as the main tools of this methodology. Starting from three different sets of acceleration FFT spectra measured on the pump casing (3-8-5 positions), the whole pump vibration characteristics were evaluated by means of a simplified FE model and the emitted noise was calculated by means of vibroacoustic BEM analyses at three different working conditions. For each set of the starting vibratory boundary conditions, this methodology was validated by comparing numerical sound power spectra with the experimental spectra obtained from sound intensity measurements. The comparison was extended to three different pump working conditions. The accuracy of the numerical results based on three experimental acceleration spectra (set 1) turned out to be not very satisfactory as the differences between experimental and numerical results were about 10 dB, on average. On the contrary, the numerical results based on eight experimental acceleration spectra (set 2) were very satisfactory. Numerical and experimental overall sound power levels always showed a very good match, irrespective of the working conditions, with differences ranging from 0 dB (configuration A) to 4 dB (configuration C).

Finally, the numerical results based on five experimental acceleration spectra (set 3) confirmed the reliability of this methodology but very significant differences between experimental and numerical results were found for configuration C, making this choice unsatisfactory for the study purposes. Due to the restricted number of cases analysed, however, these results cannot be generalised. Other investigations are in progress taking into considerations further operating and vibratory boundary conditions in order to reinforce the consistency of the validation.

References

1. Bériot H., Prinn A., Gabard G. (2013), *On the performance of high-order FEM for solving large scale industrial acoustic problems*, Proceedings of 20th International Congress on Sound and Vibration ICSV20, pp. 1–8, Bangkok.
2. Bonanno A., Pedrielli F. (2008), *A study on the structure-borne noise of hydraulic gear pumps*, Proceedings of the 7th JFPS International Symposium on Fluid Power, pp. 641–646, Toyama.
3. Borghi M., Milani M., Paltrinieri F., Zardin B. (2005), *Studying the axial balance of external gear pumps*, SAE Technical Paper 2005-01-3634.
4. Borghi M., Milani M., Paltrinieri F., Zardini B. (2008), *External gear pumps and motors bearing blocks*

design: influence on the volumetric efficiency, Proceedings of the 51st National Conference on Fluid Power, pp. 557–571, Las Vegas.

5. Carletti E., Pedrielli F. (2005), *Sound power levels of hydraulic pumps using sound intensity techniques: towards more accurate values?,* Proceedings of 12th International Congress on Sound and Vibration ICSV12, pp. 1247–1254, Lisbon.
6. Carletti E., Pedrielli F. (2006), *Measurement uncertainties in the sound power procedures based on sound intensity*, Proceedings of 13th International Congress on Sound and Vibration ICSV13, pp. 1–8, Vienna.
7. De Borst R., Crisfield M.A., Remmers J.C., Verhoosel C.V. (2012), N*on-linear finite element analysis of solids and structures*, 2nd edition, John Wiley & Sons, Chichester.
8. Huang J.K., Chang R.W., Lian Ch.W. (2008), *An optimization approach to the displacement volumes for external gear pumps*, Materials Science Forum, **594**, 57–71.
9. ISO 9614-1 (1993), *Acoustics – Determination of sound power levels of noise sources using sound intensity – Part 1: Measurement at discrete points.*
10. ISO 9614-2 (1996), *Acoustics – Determination of sound power levels of noise sources using sound intensity – Part 2: Measurement by scanning.*
11. ISO 9614-3 (2002), *Acoustics – Determination of sound power levels of noise sources using sound intensity – Part 3: Precision method for measurement by scanning.*
12. ISO 16902-1 (2002), *Hydraulic fluid power – Test code for the determination of sound power levels of pumps using sound intensity techniques: Engineering method – Part 1: Pumps.*
13. Kuang J., Lin A. (2002), *Theoretical aspects of torque responses in spur gearing due to mesh stiffness variation*, Mechanical Systems and Signal Processing, **17**, 2, 255–271.
14. Liping C., Yan Z., Fanli Z., Jianjun Z., Xianzhao T. (2011), *Modelling and simulation of gear pumps based on Modelica/MWorks*, Proceedings of 8th Modelica Conference, Dresden.
15. Manring N.D., Kasaragadda S.B. (2003), *The theoretical flow ripple of an external gear pump*, Transactions of the ASME, **125**, 396–404.
16. Margetts L. (2015), *Survey of computing platforms for engineering simulation*, NAFEMS Benchmark Magazine, 1st issue, 10–14.
17. Miccoli G., Nizzoli T., Bertolini C. (2012), *BEM & FEM-IFEM modeling and analysis methods for high complexity vehicle models*, Proceedings of the International Conference on Noise and Vibration Engineering (ISMA), pp. 4145–4158, Leuven.
18. Mucchi E., Dalpiaz G., Rincolin F. (2010a), *Elasto-dynamic analysis of a gear pump. Part I: pressure distribution and gear eccentricity*, Mech Syst Signal Process, **24**, 2160–2179.
19. Mucchi E., Dalpiaz G., Rivola A. (2010b), *Elasto-dynamic analysis of a gear pump. Part II: meshing phenomena and simulation results*, Mech Syst Signal Process, **24**, 2180–2197.
20. Mucchi E., Dalpiaz G., Rivola A. (2011), *Dynamic behaviour of gear pumps: effect of variations in operational and design parameters*, Meccanica, **46**(6), 1191–1212.
21. Mucchi E., Rivola A., Dalpiaz G. (2014), *Modelling dynamic behaviour and noise generation in gear pumps: procedure and validation*, Applied Acoustics, **77**, 99–111.
22. Opperwall T., Vacca A. (2014), *A combined FEM/BEM model and experimental investigation into the effects of fluid-borne noise sources on the air-borne noise generated by hydraulic pumps and motors*, Journal Mechanical Engineering Science, **228**(3), 457–471.
23. Parise G., Miccoli G., Carletti E. (2015), *External gear pump noise field prediction by harmonic response and vibroacoustic analyses*, Proceedings of the 22st International Congress on Sound and Vibration ICSV22, pp. 1–8, Florence.
24. Pedrielli F., Carletti E. (2005), *Investigation on standardised sound intensity methods for the determination of the sound power level of hydraulic pumps*, Proceedings of Forum Acusticum, pp. 2585–2590, Budapest.
25. Pedrielli F., Carletti E. (2014), *Acoustical evaluation of power skiving gears for hydraulic pumps*, Proceedings of the 21st International Congress on Sound and Vibration ICSV21, pp. 1–8, Beijing.
26. Ragunathan C., Manoharan C. (2012), *Dynamic analysis of hydrodynamic gear pump performance using design experiments and operational parameters*, IOSR Journal of Mechanical and Civil Engineering, **1**(6), 17–23.
27. Raju M.P., Khaitan S.K. (2012), *High performance computing of three-dimensional finite element codes on a 64-bit machine*, Journal of Applied Fluid Mechanics, **5**(2), 123–132.
28. Rodionov L., Pomatilov F., Rekadze P. (2015), *Exploration of acoustic characteristics of gear pumps with polymeric pinion shafts*, Procedia Engineering, **106**, 36–45.
29. Sandberg G., Ohayon R. (2009), *Computational aspects of structural acoustics and vibration*, Springer, New York.
30. Skaistis S. (1988), *Noise control of hydraulic machinery*, Marcel Dekker Inc., New York.
31. Stryczek J., Antoniak P., Jakhno O., Kostyuk D., Kryuchkov A., Belov G., Rodionov L. (2015) *Visualisation research of the flow processes in the outlet chamber-outlet bridge-inlet chamber zone of the gear pumps*, Archives of Civil and Mechanical Engineering, **15**, 1, 95–108.
32. Stupa V.I., Chernyshov Yu.A. (1990), *Dependence of gear-pump operation on viscosity of the metered liquid*, Chemistry and Technology of Man-Made Fibres, **21**(6), 453–455.
33. Sung-Hoon K., Hye-Min S., Jae-Cheon L. (2013), *The effect of eccentricity between gear and housing in involute gear pump*, Journal of the Korean Society of Marine Engineering, **6**, 631–637.
34. Vansant K., Bériot H., Bertolini C., Miccoli G. (2014), *An update and comparative study of acoustic modeling and solver technologies in view of pass-by noise simulation*, SAE Int. Journal Engines, **7**, 3, 1–17.
35. Wojnarowski J., Onishchenko V. (2003), *Tooth wear effects on spur gear dynamics*, Mechanism and Machine Theory, **38**, 161–178.